ASSESSING FIBRE KINEMATICS IN DILUTE FIBRE SUSPENSIONS WITH NON-NEWTONIAN SUSPENDING FLUIDS USING FAST X-RAY TOMOGRAPHY AND 3D FINITE ELEMENT SIMULATIONS

T. Laurencin[1,2,3], L. Orgéas[1], P.J.J. Dumont[2], P. Laure[3,4], S. Rolland du Roscoat[1], L. Silva[4], S. Le Corre[5], M. Terrien[6]

[1]CNRS – Univ. Grenoble Alpes, 3SR Lab, 1270 Rue de la Piscine, 38400 St Martin d'Hères, France
[2]CNRS – INSA de Lyon, LaMCoS, 18-20 rue des Sciences - F-69621 Villeurbanne cedex, France
[3]CNRS – Univ. Nice, Lab. J.A.Dieudonné,Parc Valrose F-06000 Nice, France
[4]Ecole Centrale de Nantes, ICI, 1 rue de la Noë F-44000 Nantes, France
[5]CNRS – Univ. Nantes, LTN, Rue Christian Pauc, BP 50609, F-44000 Nantes, France
[6]CNRS – Univ. Grenoble Alpes, LGP2, 1270 Rue de la Piscine 38610 Gières, France
Corresponding author: laurent.orgeas@3sr-grenoble.fr

Keywords: Non-newtonian fibre suspensions, X-ray microtomography, FE simulations, Jeffery

Abstract
The mechanical properties of short fibre-reinforced polymer composites largely depend on the fibre orientation which drastically changes during the forming of composites. To analyse the flow-induced microstructures changes, we conducted 3D *in situ* compression experiments using model non-Newtonian dilute fibre suspensions that were imaged by fast X-ray microtomography. In parallel, these experiments were numerically simulated with an Eulerian multi-domain FE code. The experimental evolution of the orientation and position of fibres were compared to the prediction of Jeffery's model and to numerical simulation. In most cases, the Jeffery's equation agrees well with the experimental and numerical data. However, for some fibres, deviations between the experimental and numerical results from the theoretical prediction were observed. The most probable cause of these deviations are flow confinement effects.

1. Introduction

Thanks to their specific physical and mechanical properties and cost-efficient processing, short fibre-reinforced polymer composites are widely used to produce (semi-)structural and (multi-)functional components for the aeronautic, electrical and automotive industries. Their performances are related to their fibrous microstructure, *i.e.*, shape, aspect ratio, concentration and orientation of fibres [1-3]. During processing or forming (film casting, injection moulding, compression moulding), short-fibre composites behave as fibre suspensions and exhibit a complex rheology. Indeed, the suspending fluids, which are usually non-Newtonian, flow and deform the fibrous microstructures *via* compaction, tearing and shear mechanisms, leading to complex translation, rotation and deformation of fibres. These phenomena severely alter the end-use properties of short-fibre composites. Unfortunately, these phenomena are not well characterised because of the difficulties to observe, analyse, model and simulate 3D evolving fibrous microstructures and deformation micro-mechanisms that occur at the fibre scale within the flowing non-Newtonian suspending fluids.
All current models which describe the kinematics of fibres in polymer composites during their forming are based on Jeffery's model prediction [4]. However, this model is only valid for a single ellipsoidal rigid particle immersed in an infinite incompressible Newtonian fluid flowing at low Reynolds number. To the best of our knowledge, this pioneering work has not been extended to the case of shear thinning suspending fluids, *i.e.*, one of the key features of the rheological properties of polymer matrices that are used in composites. For a slender ellipsoid i the orientation of which is given by the unit vector

Excerpt from ISBN 978-3-00-053387-7

$$\mathbf{p}^i = \sin\theta^i \cos\varphi^i \mathbf{e}_1 + \sin\theta^i \sin\varphi^i \mathbf{e}_2 + \cos\theta^i \mathbf{e}_3 \quad \left(\theta^i \epsilon [0,\pi] \text{ and } \varphi^i \epsilon [0,2\pi]\right), \tag{1}$$

the Jeffery's model assumes that the velocity $\mathbf{v}^i$ of the ellipsoid centre of mass is an affine function of the macroscale velocity gradient $\boldsymbol{\nabla}\mathbf{v}$ of the suspending fluid. In the absence of rigid body motion, the position $\mathbf{x}^i$ of the centre of mass of the particle can be determined by integrating the equation:

$$\mathbf{v}^i = \boldsymbol{\nabla}\mathbf{v} \cdot \mathbf{x}^i. \tag{2}$$

Besides, the evolution of the orientation the ellipsoid is predicted by integrating the following well-known expression for the rotation of $\mathbf{p}^i$:

$$\dot{\mathbf{p}}^i = \boldsymbol{\Omega} \cdot \mathbf{p}^i + \lambda \left(\mathbf{D} \cdot \mathbf{p}^i - \left(\mathbf{p}^i \cdot \mathbf{D} \cdot \mathbf{p}^i\right)\mathbf{p}^i\right), \tag{3}$$

where $\boldsymbol{\Omega} = (\boldsymbol{\nabla}\mathbf{v} - {}^t\boldsymbol{\nabla}\mathbf{v})/2$ and $\mathbf{D} = (\boldsymbol{\nabla}\mathbf{v} + {}^t\boldsymbol{\nabla}\mathbf{v})/2$ are the macroscale rotation rate and strain rate tensors, respectively, and where λ is the ellipsoid shape factor. The relevance of Jeffery's model for Newtonian fluids was experimentally confirmed by several authors [5-7], mainly for shear flow using 2D observations. Jeffery's equation was extended for axisymmetric particles by Brenner [8]. For cylindrical particles of length l and diameter d, *i.e.*, similar to fibres that are used in composites, λ is a function of the fibre aspect ratio $r = l/d$:

$$\lambda = 1 - \frac{3C \ln r}{4\pi r^2} \tag{4}$$

where C is a constant (C=5.45), the value of which was determined by Cox [9] and Anczurowski and Mason [10].

Combining (i) rheometry experiments conducted in a synchrotron X-ray microtomograph and (ii) 3D FE numerical simulation, the objective of this study was to assess the relevance of Jeffery's theory for the prediction of the flow of dilute fibre suspensions with non-Newtonian suspending fluids.

2. Materials and Methods

2.1. Materials

We prepared model fibre suspensions using a hydrocarbon gel (paraffin) as suspending fluid [11]. Its transparency enabled us to control the fibre placement during the suspension preparation. The viscosity of this gel was easily adjusted by varying the temperature. At 120°C, the gel behaved as a Newtonian fluid and its shear viscosity was about 1 Pa s. At room temperature, the gel was solid, which enabled us to "freeze" the fibrous microstructure of the suspensions. At 50°C, the gel exhibited a non-Newtonian behaviour close to that of industrial polymers used for composites: the shear viscosity of the gel μ followed a shear-thinning power-law, *i.e.*, $\mu = K\dot{\gamma}^{n-1}$, where $\dot{\gamma} = \sqrt{2\mathbf{D}:\mathbf{D}}$ was the generalised shear rate and the power-law exponent $n = 0.2$ as well as the consistency $K = 438$ Pa s^{1-n} were determined using rheometry experiments (cone-plate rheometer, Anton Paar MCR301). Fibres used as reinforcements were extracted from a continuous elastic fishing wires (diameter 200 µm) which presents a sufficiently different X-ray absorption coefficient with the matrix. To process fibre model suspension, fibres were cut at a constant length l from continuous wire with a razor blade to obtain a desired aspect ratio $r = l/d$ length and blunt-ended extremities. The suspensions were hand-made layer by layer while keeping the control of the fibre orientation. The process consists in picking fibres in a thin layer a solid gel with desired orientations and impregnate fibres with a second layer of pre-heated gel at 120°C. Suspensions were fabricated in cylindrical moulds (radius 7 mm, height 5 mm).

2.2. Rheometry with 3D Imaging

Then, the as-prepared suspensions were compressed in a dedicated micro-rheometer which enabled simple compression tests at various strain and strain rates to be conducted. Heaters and thermocouples were installed under the compression platens so as to maintain the samples at a constant temperature of 45°C. The compression cell was made of PMMA, *i.e.*, a material with a low absorption of X-rays.

Excerpt from ISBN 978-3-00-053387-7

The mechanical loading was continuously applied via a piezoelectric linear actuator. The micro-rheometer was especially designed and mounted on the rotation stage of a synchrotron X-ray microtomograph (Swiss Light Source, Tomcat beamline, Villigen, Switzerland, energy of 20 keV, voxel size of 11 μm^3, scanning time of 0.42 s), enabling us to take original real-time 3D images of the evolving microstructure of studied suspensions during compression as shown for example in Fig. 1(a). Compression tests were conducted at constant compression platen velocity of 155 $\mu m\, s^{-1}$ so as to reach a compression Hencky strain $\varepsilon_{33} = \ln(h/h_0) \approx -0.45$ (where h_0 and h are the initial and current heights of the tested suspension, respectively).

2.3. Image Analysis

Dedicated image analysis was performed on X-ray images to extract time-dependent positions and orientations of fibres in the suspensions. The methodology was similar to that proposed by Latil *et al.* [12]. Fibre centrelines were obtained from a skeletonisation algorithm, namely the distance-ordered homotopic thinning [13] implemented in the Avizo software. The shape of fibres was characterised with a local Frenet basis, containing the tangent, normal and binormal unit vectors defined along the curvilinear abscissa of fibres. The rigid motion of fibres was tracked by using a particle tracking algorithm based on discrete correlation distance functions [14]. This procedure enabled the evolution of the centre of mass $\mathbf{x}_{exp}^i$ and the orientation $\mathbf{p}_{exp}^i$ of each fibre i of the suspension to be detected, as well as the relevance of the Jeffery's model to be assessed: affine motion of fibre mass centre, rigid motion of fibres, and orientation Jeffery-based models. For that purpose, Eqs. (2-3) were numerically integrated using the Runge-Kutta fourth order scheme ode45 that was implemented in Matlab. Thus, for each fibre, the initial experimental positions of the centre of mass and orientation vectors of fibres were used as integration input data. Besides, it was verified that the flow was homogeneous and incompressible ($\boldsymbol{\nabla} \cdot \mathbf{v} = 0$ [11]). The flow was also assumed to be rotation free ($\boldsymbol{\Omega} = 0$). Finally, the strain rate tensor $\mathbf{D}$ was calculated using the actual height of the suspension h which was measured using 3D images.

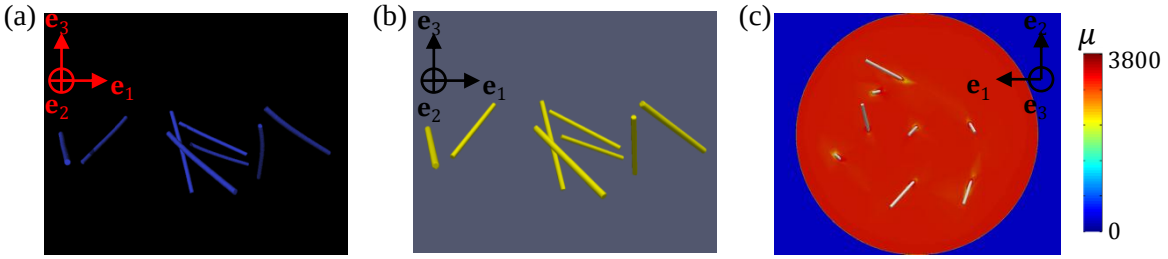

Figure 1. 3D images of the experimental (a) and numerical (b) fibrous phase at a compression Hencky strain ε_{33} of -0.2. (c) Isovalues of the local viscosity μ in a fixed $(\mathbf{e}_1, \mathbf{e}_2)$ plane.

2.4. Finite Element Simulations

The experiments were also simulated using a Finite Element (FE) code [15] based on a multi-domain approach and an Immersed Volume method. This approach was implemented to embed one Eulerian mesh on all domains. Therefore, a level-set function was associated to each subdomain (air, compression platens, fluid, fibres). By using Heaviside functions, material parameters (density, viscosity and so on) were defined on the entire domain and led to the formulation of a multiphase Stokes system of equations. Velocity and pressure in the entire computational domain were computed with the FE method through the resolution of momentum and mass conservation equations [15]. However, a Lagrange multiplier linked to the rigidity condition inside fibre was added to the classical formulation [16].This code has already been used to study the flow of Newtonian suspensions of rigid fibres and spheres [16-17]. In our calculations, fibres were considered to be rigid and straight. Besides, in accordance with the rheology of the hydrocarbon gel, the shear viscosity of the fluid phase μ followed a shear-thinning power-law, *i.e.*, $\mu = K\dot{\gamma}^{n-1}$. To run the simulations, we also added a

Excerpt from ISBN 978-3-00-053387-7

viscous layer between the suspensions and the compression platens. The viscosity μ_l of this layer was adjusted to reproduce possible friction effects, *i.e.*, from no-slip to perfect slip boundary conditions. Numerical simulation was first performed only on the suspending fluid to verify the ability of the code to reproduce purely elongational flow for Newtonian and non-Newtonian fluids and to fit well-known analytical solutions [18]. Best results were obtained for air and viscous layers with viscosities $\mu_a = \mu_l = 10^{-3}\max(\mu)$ and for mould and fibre "viscosities" $\mu_m = \mu_f = 10^{3}\max(\mu)$. Then, simulations were performed on fibre suspensions. For that purpose, the fibre descriptors that were experimentally determined at the initial state of compression were used as initial geometrical input data for numerical 3D simulation. Typical simulation results are shown in Fig. 1(b-c). The numerical simulation enables to both compute and extract $\mathbf{x}_{num}^{i}$ and the orientation $\mathbf{p}_{num}^{i}$ of each fibre i during suspension flow, and the fibre scale stress and strain rate fields.

3. Results and Discussion

Three experiments were conducted and their results were compared with both the theoretical and numerical predictions: the first tested suspension contained one fibre ($r = 19.5$), the second had five fibres ($r = 12.5$) and the third had eight fibres ($r = 19.5$). Corresponding results are shown in Figs. 2-4 where graphs (a) and (b) give the evolution with the compression strain $|\varepsilon_{33}|$ of the orientation angles θ^i and φ^i of each fibre i, respectively. In addition, graphs (c) show the evolution with the compression strain ε_{33} of the experimental and numerical dispersions, which were defined as $\Delta x_{exp}^{i} = \|\mathbf{x}_{exp}^{i} - \mathbf{x}_{Jeff}^{i}\|/h_0$ and $\Delta x_{num}^{i} = \|\mathbf{x}_{num}^{i} - \mathbf{x}_{Jeff}^{i}\|/h_0$, respectively, with respect to the affine motion assumption Eq.(2) of Jeffery's theory.

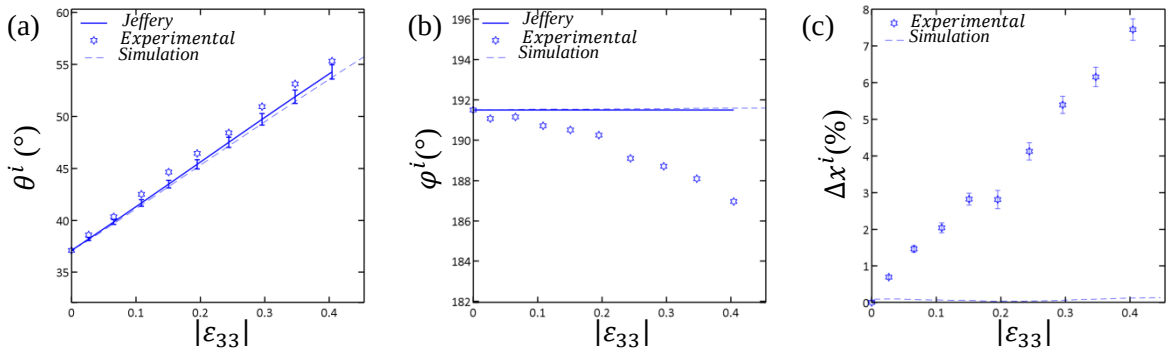

Figure 2. Compression test results obtained for a suspension containing one fibre. Experimental, numerical and theoretical evolutions of the angles θ^i (a) and φ^i (b) with $|\varepsilon_{33}|$. Experimental and numerical evolutions of dispersions Δx_{exp}^{i} and Δx_{num}^{i} with $|\varepsilon_{33}|$.

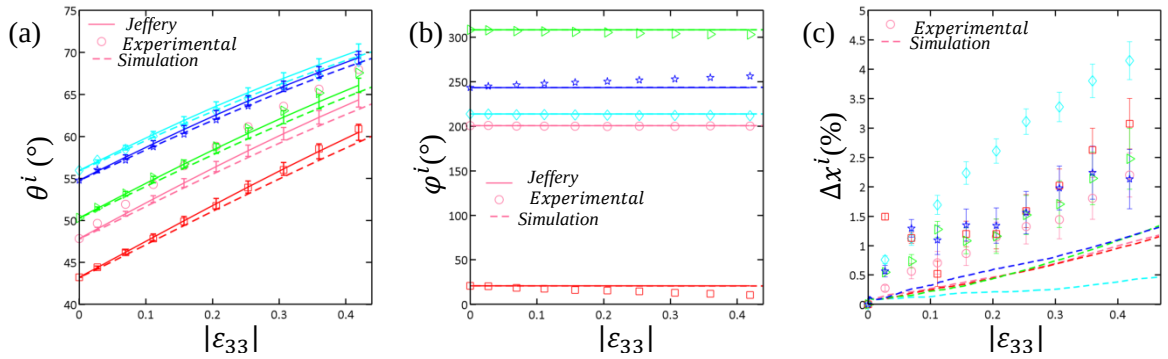

Figure 3. Simple compression test results obtained for a suspension containing five fibres. Experimental, numerical and theoretical evolutions of the angles θ^i (a) and φ^i (b) with $|\varepsilon_{33}|$. Experimental and numerical evolutions of dispersions Δx_{exp}^{i} and Δx_{num}^{i} with $|\varepsilon_{33}|$.

Excerpt from ISBN 978-3-00-053387-7

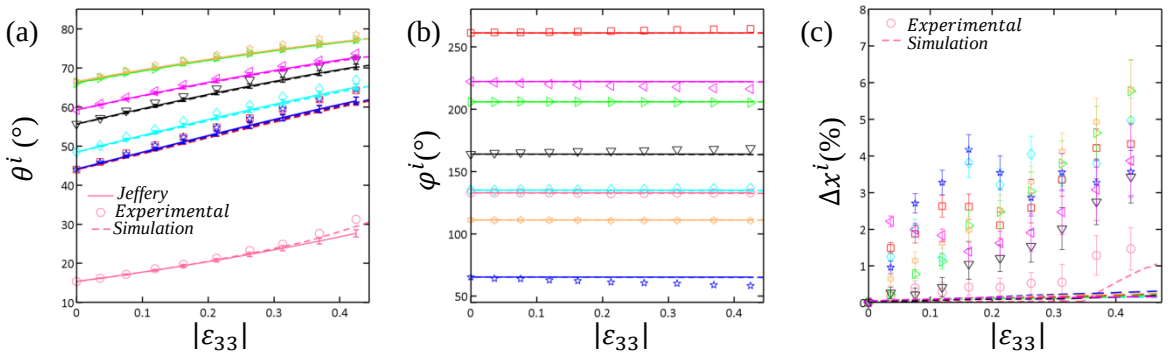

Figure 4. Simple compression test results for a suspension containing eight fibres. Experimental, numerical and theoretical evolutions of the angles θ^i (a) and φ^i (b) with $|\varepsilon_{33}|$. Experimental and numerical evolutions of dispersions Δx^i_{exp} and Δx^i_{num} with $|\varepsilon_{33}|$.

The following comments can be made on these figures:

- Regardless of the experimental conditions, fibres tended to align along the $(\mathbf{e}_1, \mathbf{e}_2)$ plane, perpendicular to the compression direction $\mathbf{e}_3$: the angles θ^i increased with ε_{33} and tended to reach a value of $\pi/2$ (graphs (a)). In addition, the rotation of fibres in the $(\mathbf{e}_1, \mathbf{e}_2)$ plane was close to zero: the angles φ^i remained practically constant (graphs (b)). Lastly, the motion of the centre of mass of each fibre was rather close to the affine motion assumption: the experimental dispersions remained below 10% (see graphs (c)).
- The graphs of Figs. 2-4 show the numerical predictions were in very good accordance with the experimental results. Indeed, predicted orientation angles fairly well fitted those that were experimentally recorded. Besides, departures of the translation of fibres from the affine solutions were very weak and followed the experimental trends (the dispersions Δx^i_{num} were always below Δx^i_{exp}, the experimental dispersions being less accurate because of experimental artefacts). These results tend to validate the numerical code as a proper simulation tool to conduct numerical fine scale rheometry.
- Figs. 2-4 also clearly show that most of experimental and numerical results were very well-fitted by the Jeffery's theory. Depsite the highly shear thinning behaviour of the suspending fluid, both the evolution of the fibre orientations and the fibre positions were well-captured by the analytical Jeffery's estimates. Thus, two conclusions can be drawn. First, the non-Newtonian nature of the purely viscous fluid did not have primary effects on the kinematics of fibres, at least for the investigated testing conditions. Second, for suspensions with several fibres such as those studied in Figs.3-4, where the distances between fibres were of the order of the fibre length l, long range hydrodynamics interactions between fibres remained weak and did not have any strong influence on the fibre kinematics. The slice plotted in Fig.1(c) higlights this point: the numerical results showed that high strain rate gradient zones were located in the vicinity of fibres, *i.e.*, in zones of thicknesses close to that of the fibre diameter d.
- Numerical and (in a less tangible way) experimental results also showed some interesting effects, such as the role of flow confinement effects on the fibre kinematics. This effect was apparent for the fibre with pink marks in Fig. 4. Above $\varepsilon_{33} = -0.3$, one extremity of this fibre was nearly in contact with one of the compression platens up to the end of the test. During this stage, both the fibre orientation and motion were affected by the platen and significantly deviated from Jeffery's prediction (Fig.4 (a,c)).

Excerpt from ISBN 978-3-00-053387-7

4. Conclusion

We studied the rheology of model dilute fibre suspensions with a non-Newtonian suspending fluid, by combining both fine scale FE numerical simulation and micro-rheometry experiments with 3D *in situ* observations of the evolving fibrous microstructures. These two methods were shown to be particularly well-suited to analyse fibre kinematics in these complex systems. When fibres were not in close contact with compression platens, we showed that Jeffery's theory and its related affine assumptions led to proper estimates of the orientation and motion of fibres within the studied non-Newtonian viscous suspensions. This interesting result must be confirmed for higher fibre concentrations. We also observed confinement effects when fibres were in the vicinity of compression platens. These effects drastically affected the fibre kinematics and should be taken into account in rheological models.

Acknowledgements

Tanguy Laurencin gratefully acknowledges the LabEx Tec21 (Investissements d'Avenir - grant agreement n°ANR-11-LABX-0030) for his PhD research grant. We acknowledge the Paul Scherrer Institut, Villigen, Switzerland for provision of synchrotron radiation beamtime at beamline TOMCAT of the SLS and would like to thank Rajmund Mokso and Anne Bonnin for assistance.

References

[1] S-Y. Fu, B. Lauke. Effects of fiber length and fiber orientation distributions on the tensile strength of short-fiber-reinforced polymers. *Elsevier Science*, 56:1179-1190, 1996.
[2] M. Djalili-Moghaddam, S. Toll. Fibre suspension rheology: effect of concentration, aspect ratio and fibre size. *Rheologica Acta*, 45:315-320, 2006.
[3] S.G. Advani. Flow and rheology in polymer composites manufacturing. *Elsevier Science*, 10,1994.
[4] G.B. Jeffery. The motion of ellipsoidal particles immersed in a viscous fluid. *Proceedings of the Royal Society of London A* 102, 1922.
[5] R. C. Binder. The Motion of Cylindrical Particles in Viscous Flow. *Journal of Applied Physics* 10, 711, (1939)
[6] B.J. Trevelyan, S.G. Mason. Particle motions in sheared suspensions I. Rotations, J. Colloid Sci. 6:354–367, 1951.
[7] Michael P. Petrich, Donald L. Koch. Claude Cohen. An experimental determination of the stress–microstructure relationship in semi-concentrated fiber suspensions. *Journal of Non-Newtonian Fluid Mechanics*, 95:101–133, 2000.
[8] H. Brenner. Rheology of a dilute suspension of axisymmetric Brownian particles. *International Journal of Multiphase Flow*, 1: 195-341, 1974.
[9] R. G. Cox. The motion of long slender bodies in a viscous fluid. Part 2. Shear flow, *Journal of Fluid Mechanics*. 45: 625-657, 1971.
[10] E. Anczurowski and S. G. Mason. Particle motions in sheared suspensions. XXIV. Rotation of rigid spheroids and cylinders. *Transactions of The Society of Rheology*, 12: 209-215, 1968
[11] O. Guiraud, L. Orgéas. Microstructure and deformation micromechanisms of concentrated fiber bundle suspensions: An analysis combining x-ray microtomography and pull-out tests. *Journal of Rheology*, 56(3) : 593-623, 2012.
[12] P. Latil, L. Orgéas, C. Geindreau, P.J.J. Dumont, S. Rolland du Roscoat. Towards the 3D in situ characterization of deformation micro-mechanisms within a compressed bundle of fibre. *Composites Science and Technology*, 71:480–488, 2011.
[13] C. Pudney. Distance-Ordered Homotopic Thinning: A Skeletonization Algorithm for 3D Digital Images. *Computer vision and image understandin*g, 72: 404–413, 1998.
[14] S. Le Corre, P. Latil, L. Orgéas, P.J.J. Dumont, S. Rolland du Roscoat, C. Geindreau. A 3D image analysis for fibrous microstructures: discretization and fiber tracking. *ECCM15, 15th European conference on composite materials, Venice, Italy*, 2012.
[15] T. Coupez, H. Digonnet, E. Hachem, P. Laure, L. Silva and R. Valette. Multidomain Finite Element Computations: Application to Multiphasic Problems, Arbitrary Lagrangian-Eulerian and Fluid-Structure Interaction. *Numerical Simulation, Wiley*, 221-289, 2010.

Excerpt from ISBN 978-3-00-053387-7

[16] P. Laure, G. Beaume, O. Basset, L. Silva, T. Coupez. Numerical Methods for solid particles in particulate flow simulations, Euro. *European Journal of Computational Mechanics*, 16: 365–383, 2007.
[17] V. Verdon, A. Lefebre-Lepot, P. Laure, L. Lobry. Modified Lees-Edwards boundary conditions and viscous contact for numerical simulations of particles in a shear flow. *European Journal of Computational Mechanics*, online 2012.
[18] J. Engmann, C. Servais, A. S. Burbidge. Squeeze flow theory and applications to rheometry: A review, *Journal of Non-Newtonian Fluid Mechanics,* 132**:**1-27 (2005).

Excerpt from ISBN 978-3-00-053387-7